Int. J. Heat Mass Transfer. Vol. 8, pp. 1135–1151. Pergamon Press 1965. Printed in Great Britain

BINARY DIFFUSION AND HEAT TRANSFER IN LAMINAR FREE CONVECTION BOUNDARY LAYERS ON A VERTICAL PLATE

WILLIAM N. GILL,* EDUARDO DEL CASAL† and DALE W. ZEH‡
Syracuse University, New York

(*Received* 10 *August* 1964 *and in revised form* 15 *March* 1965)

Abstract—Free convection in laminar boundary layers with coupled momentum, heat and binary mass transfer was investigated in terms of relevant parameters. Buoyancy effects caused by both temperature and concentration gradients were considered. Exact solutions of the nonlinear system of three coupled equations for variable physical property systems with a constant generating body force parallel to the solid surface were investigated for many different cases in order to get a reasonable idea of how the various parameters influence the transport processes involved.

The effects of variations in specie enthalpy, thermal conductivity, viscosity and density with concentration were studied individually and in various combinations. The most striking effects are those caused by specie enthalpy differences and thermal conductivity for the low molecular weight gases. Also the interactions of Prandtl number and interfacial velocity effects for single component mass-transfer systems were investigated.

A method of integrating the coupled transport equations was developed which appears to be substantially faster than previously used techniques. The improved speed of computation occurs primarily because each solution of the momentum equation is obtained by iterating only on a boundary condition rather than on both a boundary condition and a function as previous methods require.

NOMENCLATURE

C_p, heat capacity, [Btu/lb degF];
D_{AB}, coefficient of diffusion of component A into component B;
g, gravitational acceleration;
g_x, component of acceleration of gravity in x-direction;
g_y, component of acceleration of gravity in y-direction;
h_D, local mass-transfer coefficient;
h_H, local heat-transfer coefficient;
k, thermal conductivity;
M, molecular weight;
Nu_x, Nusselt number $(h_H x)/k$;
Pr, Prandtl number $(\mu C_p)/k$;
Sc, Schmidt number ν/D_{AB};
Sh_x, Sherwood number $(h_D x)/D_{AB}$;
T, temperature;
u, x-direction component of velocity;
v, y-direction component of velocity;
x, distance along surface;
X, mole fraction.

Greek symbols

μ, viscosity;
ν, kinematic viscosity;
ρ, density;
τ, shear stress;
ψ, stream function;
ω, mass fraction.

Subscripts

A, refers to component A;
B, refers to component B;
w, refers to conditions at $y = 0$;
∞, refers to conditions at $y = \infty$.

* Professor of Chemical Engineering, Clarkson College of Technology, Potsdam, N.Y.
† Research Specialist, Boeing Co., Seattle, Washington.
‡ N.S.F. Fellow, Ch.E. Dept., Syracuse University, Syracuse, N.Y.

IN RECENT YEARS free convection boundary layer problems have received considerable attention

because they are important in situations of practical interest and have an academic appeal as well. Since Prandtl's boundary-layer theory was originally developed to deal with high Reynolds number flows, it is interesting that this concept can be employed effectively to describe transport processes in the relatively low velocity systems often encountered in free convection when the body force is created by the gravitational field of the earth. However, flows can be created by other body forces such as Coriolis or centrifugal force fields, and in such cases rather high velocity free convection flows can exist which influence heat-transfer processes. This fact apparently provided some of the motivations for earlier studies by Eckert [2] and Ostrach [5]. Subsequently, vaporization or evaporative cooling was cited by Somers [7] as a practical application of his study of heat and mass transfer in a free convection boundary layer on a flat plate. Nakamura [4] reflects an interest in the details of the simultaneous transfer of sensible and latent heat when the material transferred is water vapor as is the case in many applications where free convection may be important. Eichhorn [3], and more recently Sparrow, Minkowycz and Eckert [10, 11] remarked on the need to protect surfaces from the effects of high temperature gas streams and thus they studied mass transfer cooling in free convection stagnation flows.

A variety of solutions dealing with variations on the single component fluid, constant fluid property and surface temperature theme are available in the literature [1, 5, 6, 8, 13]. Also, rather small first-order perturbations on the boundary-layer theory have been calculated [12]. Studies by Somers [7] and Nakamura [4] deal with the problem of simultaneous heat transfer and binary diffusion. However, both of these authors investigated only a limited range of parameters, assumed constant physical properties and neglected the effects of specie enthalpy differences. Also, Somers employed only an approximate integral method and Nakamura neglected buoyancy forces caused by concentration distributions. As a consequence of Nakamura's assumptions, all his results, except concentration distributions for $N_{Sc} = 0{\cdot}5$, $0{\cdot}6$, were obtained almost simultaneously by Eichhorn [3], and later extended regarding surface temperature distribution [9].

Very recently Sparrow, Minkowycz and Eckert [10, 11] studied in detail various effects which occur in several binary systems consisting of air mixtures. They included thermal diffusion and diffusion thermo in their analysis of free convection stagnation flow and showed that coupling phenomena can be significant. Furthermore, their study reported the interesting result that if coupling effects are neglected, then, in certain mixtures, with stream temperatures, say, $T_w/T_\infty \simeq 1{\cdot}1$, mass transfer can increase the heat flux by as much as 70 per cent over the case with no mass transfer.

Although much has been written about single component free convection boundary layers, there is a relative dearth of information about the influence of such important parameters as Prandtl number, Schmidt number and physical property effects on binary systems. In the present study, a rather wide range of parameters, which represents both gaseous and liquid two component systems, it investigated. Since this investigation deals with a multi-parameter problem, and each solution obtained is for a system of three coupled nonlinear equations, it is not feasible to cover all possible cases of interest. Consequently, an attempt has been made to obtain a sufficient number of solutions so that one can assess the importance of each parameter and to include representative cases which give a reasonable picture of how different variables affect free convection in gases and liquids.

In addition to the physical motivation for this study, there was a desire to develop a more rapid method of solving the involved transport equations. Methods used to date are quite time consuming, even when the fastest of currently available high-speed computers are used. This, coupled with the fact that the number of parameters relevant to the problem is very large, serves to dampen enthusiasm for detailed studies of the variable property boundary layer.

ANALYSIS

The problem studied, as sketched in Fig. 1, is that of free convection over a vertical plate, wherein the buoyancy forces arise due to the existence of both temperature and concentration

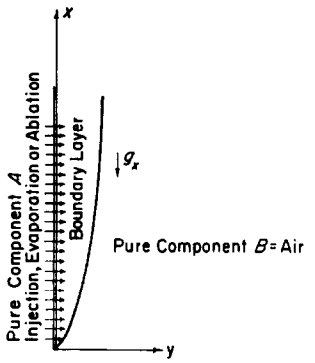

FIG. 1. Vertical flat surface with free convection induced by both temperature and concentration gradients.

gradients, the latter being sustained by interfacial mass transfer.

If Soret–Dufour diffusion, viscous dissipation and work of compression are neglected, the boundary-layer equations for non-reacting systems are:

Continuity:

$$\frac{\partial(\rho u)}{\partial x} + \frac{\partial(\rho u)}{\partial y} = 0 \tag{1}$$

Momentum:

$$\rho u \frac{\partial u}{\partial x} + \rho v \frac{\partial u}{\partial y} = \frac{\partial}{\partial y} \mu \frac{\partial u}{\partial y} - \frac{\partial p}{\partial x} + \rho g_x \tag{2}$$

Energy:

$$C_p \left[\rho u \frac{\partial T}{\partial x} + \rho v \frac{\partial T}{\partial y} \right] = \frac{\partial}{\partial y} k \frac{\partial T}{\partial y} + \rho D (C_{p_A} - C_{p_B}) \frac{\partial T}{\partial y} \frac{\partial \omega_A}{\partial y} \tag{3}$$

Diffusion:

$$\rho u \frac{\partial \omega_A}{\partial x} + \rho v \frac{\partial \omega_A}{\partial y} = \frac{\partial}{\partial y} \rho D \frac{\partial \omega_A}{\partial y} \tag{4}$$

with the boundary conditions

at $y = 0$: $u = 0$, $v = v_w = -\dfrac{D}{1 - \omega_{A_w}} \dfrac{\partial \omega_A}{\partial y}\Big|_w$

$T = T_w$, $\omega_A = \omega_{A_w}$, both constant.

at $y = \infty$: $u = 0$

$T = T_\infty$, $\omega_A = 0$

For this case, $g_x = -g$ and by letting $y \to \infty$ in equation (2), we see that within the boundary-layer approximations the pressure gradient is given by

$$-\frac{\partial p}{\partial x} = \rho_\infty g \tag{5}$$

The continuity equation is satisfied by defining the stream function ψ as

$$u \Lambda_\rho = \frac{\partial \psi}{\partial y}, \quad v \Lambda_\rho = -\frac{\partial \psi}{\partial x} \tag{6}$$

where $\Lambda_\rho = \rho/\rho_\infty$. Equations (2), (3) and (4) may be reduced to total differential form by utilizing equations (5) and (6) and defining the following variables:

$$\eta = \left[\frac{g}{4\nu_\infty^2 x}\right]^{1/4} \int_0^y \Lambda_\rho^a \Lambda_\mu^e \, dy, \quad \psi = 2(2)^{1/2} [g x^3 \nu_\infty^2]^{1/4} F(\eta)$$

$$\theta = \frac{T - T_\infty}{T_w - T_\infty}, \quad \phi = \frac{\omega_A}{\omega_{A_w}}$$

This yields

Momentum:

$$\frac{d}{d\eta}\left[\Lambda_\rho^a \Lambda_\mu^{e+1} \frac{d}{d\eta}\left(\Lambda_\rho^{a-1} \Lambda_\mu^e \frac{dF}{d\eta}\right)\right] + 3F \frac{d}{d\eta}\left(\Lambda_\rho^{a-1} \Lambda_\mu^e \frac{dF}{d\eta}\right) - 2\Lambda_\rho^{a-1} \Lambda_\mu^e \left(\frac{dF}{d\eta}\right)^2 + \Lambda_\rho^{-a} \Lambda_\mu^{-e} (1 - \Lambda_\rho) = 0 \tag{7}$$

Energy:

$$\frac{d}{d\eta}\left(\Lambda_k \Lambda_\rho^a \Lambda_\mu^e \frac{d\theta}{d\eta}\right) + Pr_\infty \left[3\Lambda C_p F + \omega_{A_w} \frac{C_{p_A} - C_{p_B}}{C_{p_\infty}} \Lambda_\rho^{a+1} \Lambda_\mu^e \Lambda_D \frac{d\phi}{d\eta}\right] \frac{d\phi}{d\eta} = 0 \tag{8}$$

Diffusion:

$$\frac{d}{d\eta}\left(\Lambda_D \Lambda_\rho^{a+1} \Lambda_\mu^e \frac{d\phi}{d\eta}\right) + 3Sc_\infty F \frac{d\phi}{d\eta} = 0 \tag{9}$$

where $\Lambda_{C_p} = C_p/C_{p_\infty}$, $\Lambda_D = D/D_\infty$. The choice of values for (d, e) is entirely arbitrary but the present authors found that for computational purposes it was convenient to let $(d, e) = (0, -1)$. Then for equations (7), (8) and (9) respectively, if primes denote differentiation with respect to η, one gets

$$\left(\frac{F'}{\Lambda_\mu \Lambda_{\rho_c}}\right)'' + 3F\left(\frac{F'}{\Lambda_\mu \Lambda_{\rho_c}}\right)' - 2\frac{(F')^2}{\Lambda_\mu \Lambda_{\rho_c}} + \Lambda_\mu \Lambda_{\rho_c}(\Lambda_{\rho_{ct}}^{-1} - 1) = 0 \qquad (10)$$

$$\left(\theta' \frac{\Lambda_k}{\Lambda_\mu}\right)' + Pr_\infty\left[3\Lambda_{C_p} F + \frac{C_{p_A} - C_{p_B}}{Sc\ C_{p_\infty}} \omega_{A_w} \phi'\right] \theta' = 0 \qquad (11)$$

$$\left(\frac{\phi'}{Sc}\right)' + 3F\phi' = 0 \qquad (12)$$

with the boundary conditions

$$F(0) = \tfrac{1}{3}\frac{\omega_{A_w}}{1 - \omega_{A_w}} Sc_w\, \phi'(0),\ F'(\infty) = 0,\ F'(\infty) = 0$$

$$\theta(0) = 1,\quad \theta(\infty) = 0$$

$$\phi(0) = 1,\quad \phi(\infty) = 0$$

The important dimensionless transport quantities are

$$Nu_x = -\left[\frac{gx^3}{4\nu_\infty^2}\right]^{1/4} \frac{\Lambda_{k_w}}{\Lambda_{\mu_w}} \theta'(0)$$

$$Sh_x = -\left[\frac{gx^3}{4\nu_\infty^2}\right]^{1/4} \Lambda_{Sc_w}^{-1} \phi'(0)$$

$$\frac{\tau_w x^2}{\nu_\infty \mu_\infty} = 4\left[\frac{gx^3}{4\nu_\infty^2}\right]^{3/4} \Lambda_{\nu_w}^{-1} F''(0)$$

In this study the quantities $\Lambda_\rho \Lambda_\mu$, Λ_k/Λ_μ and Λ_{c_p} were assumed to be temperature independent (to denote this, the quantity Λ_ρ is subscripted with a "c" when it appears in a product with Λ_η, and with a "ct" when it is considered as a function of both temperature and concentration). Indeed, these are successful assumptions in studies of single-component gaseous systems. As pointed out in later discussion, the validity of these assumptions in the present case is demonstrated in Fig. 2.

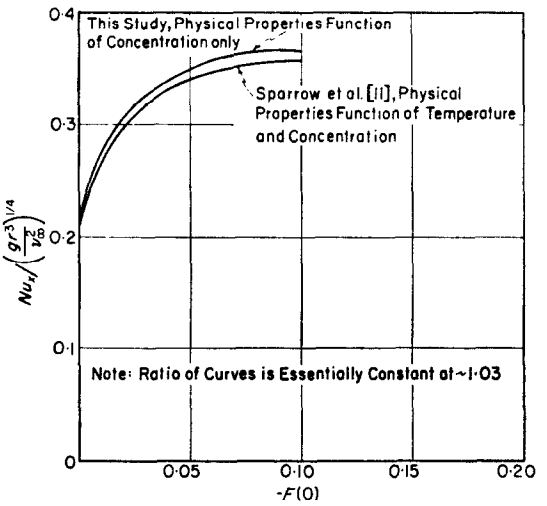

FIG. 2. Heat-transfer rate vs. blowing parameter. Comparison of results of present study (physical properties only concentration dependent) with those of Sparrow *et al.* (physical properties concentration and temperature dependent) for a helium–air system in free convection stagnation flow. $T_w/T_\infty = 1{\cdot}1$.

For the special case of a single-component gaseous system, we may write

$$\Lambda_\rho^{-1} = \left(\frac{T_w}{T_\infty} - 1\right)\theta + 1$$

Then, by redefining the transformation variables as

$$\eta = \left[\left(1 - \frac{T_w}{T_\infty}\right)\frac{gx}{4\nu_\infty^2}\right]^{1/4} y,$$

$$F = \frac{\psi}{4\nu_\infty\left[\left(1 - \frac{T_w}{T_\infty}\right)\frac{g_x x^3}{4\nu_\infty^2}\right]^{1/4}}$$

Equations (10) and (11) become

$$F''' + 3FF'' - 2(F')^2 + \theta = 0 \qquad (13)$$

$$\theta'' + 3Pr\, F\theta' = 0 \qquad (14)$$

Hence, the results obtained for the single-component system are independent of (T_w/T_∞). The

important dimensionless transport quantities are

$$\frac{\tau_w x^2}{\nu\mu} = (4\,Gr_x^3)^{1/4} F''(0)$$

$$Nu_x = -\left(\frac{Gr_x}{4}\right)^{1/4} \theta'(0)$$

where the Grashof number is given by

$$Gr_x = \left(1 - \frac{T_w}{T_\infty}\right)\frac{g}{\nu_\infty^2}\chi^3$$

As mentioned in the introduction, this case has been treated by other workers, but not in detail, and so further information is presented herein.

Also included in this analysis was a two component liquid system, with $Pr_\infty = 10$, $Sc_\infty = 500$. With such a large value for the Schmidt number, it may be assumed that the diffusion boundary layer is sufficiently thin that property variation with concentration and free convection due to concentration gradients may be ignored. If one then assumes

$$\frac{\rho_\infty}{\rho} = 1 + \beta(T - T_\infty)$$

and substitutes the quantity $\beta(T_w - T_\infty)$ for the quantity $[1 - (T_w/T_\infty)]$ in the definition of η, F and Gr_x above, then equations (12), (13) and (14) result. The additional dimensionless quantity for mass transfer is

$$Sh_x = -\left(\frac{Gr_x}{4}\right)^{1/4} \phi'(0)$$

METHOD OF SOLUTION

The equations to be solved are coupled and nonlinear with coupled boundary conditions, The general iterative process used to solve them is outlined below.

1. Assume a solution to the momentum equation, and assume
   $\Lambda_\rho \equiv \Lambda_\mu \equiv \Lambda_k \equiv \Lambda_{c_p} \equiv \Lambda_k \equiv 1$,
   $Sc = Sc_\infty$.
2. Solve the energy and diffusion equations; if Λ_ρ, Λ_μ, etc., are assumed known (initially from step 1, and in subsequent iterations from step 3) then although the equations are boundary-value in nature, they are linear and no iteration is required.
3. Evaluate Λ_ρ, Λ_μ, etc.
4. Solve the momentum equation; this is a nonlinear boundary value problem requiring an iterative process. The condition on $F'(\infty)$ must be converted to a condition on $F''(0)$:
   a. Assume $F''(0)$
   b. Integrate the momentum equation
   c. If the condition on $F'(\infty)$ is satisfied, solution is obtained, go to 5. If not, adjust $F''(0)$ and return to 4b.
5. If the solution of the momentum equation is the same as that assumed in step 1 or is the same as a solution obtained in a previous iteration at step 4, the solution is complete. If not, return to step 2.

The most common method of solving equations of the present type has been based upon implicit integral equations (e.g. [11]). A characteristic of the procedure is that in the solution of the momentum equation, i.e. step 4 above, use is made of the solution obtained in the previous iteration. For example, in the present case equation (10) would be solved in the ith iteration as

$$\left(\frac{F_i}{\Lambda_\mu\Lambda_{\rho c}}\right)'' + 3F_{i-1}\left(\frac{F_i'}{\Lambda_\mu\Lambda_{\rho c}}\right)' - 2\frac{(F_{i-1}')^2}{\Lambda_\mu\Lambda_{\rho c}} + \Lambda_\mu\Lambda_{\rho c}(\Lambda_{\rho ct}^{-1} - 1) = 0$$

where F_{i-1} and F_{i-1}' are assumed known from the previous overall iteration. Clearly, if the momentum equation is strongly temperature and concentration dependent, as it certainly is in a pure free convection problem, convergence by such a scheme will be slow.

The authors have formulated an alternate scheme which proceeds more rapidly. Letting

$$G = \frac{F'}{\Lambda_\mu\Lambda_\rho} \tag{15}$$

equation (10) becomes

$$G'' + 3FG' - 2\Lambda_{\rho c}\Lambda_{\mu}(G')^2 + \Lambda_{\mu}\Lambda_{\rho c}(\Lambda_{\rho ct}^{-1} - 1) = 0 \quad (16)$$

If a form for F is known, equation (16) may be readily solved by a direct integration scheme, such as Runge–Kutta, proceeding as outlined in step 4 above. It was found that F could be accurately approximated by a truncated Taylor series in terms of G at each step of the integration. For example, proceeding in the integration scheme from point η_1, we write

$$F(\eta) = F(\eta_1) + \int_{\eta_1}^{\eta} F'\,d\eta \simeq F(\eta_1) + (\Lambda_{\rho c}\Lambda_{\mu})_{\text{av}} (\eta - \eta_1)\left[G(\eta_1) + \frac{\eta - \eta_1}{2}G'(\eta_1) + \frac{(\eta - \eta_1)^2}{6}G''(\eta_1)\right]$$

F, G, G' and G'' are, of course, known at η_1, and an arithmetic average of $\Lambda_{\rho c}\Lambda_{\mu}$ was sufficiently accurate. Hence, there is no need to assume a form for F as we have an accurate approximate closed form representation from point to point along the path of integration.

With the present method, solution of the momentum equation is obtained by iterating only on a boundary condition rather than both a boundary condition and a function as required by the technique first described. It was found that solutions could be obtained in from 1½ to 4 min on an IBM 7074 Computer, whereas Sparrow *et al.* [11], required up to 30 min with the CD 1604 which is about ten times faster than the IBM machine. It must be remembered that the solutions obtained by Sparrow *et al.* involved calculations of much more complicated functions for the physical properties, but it is the opinion of the authors that this is not the "rate-determining step" in the solution. Also to be considered in comparing relative calculation time is the precision and accuracy required in the study by Sparrow *et al.*, which may have been greater or less than that employed here. In this study, the value of $F''(0)$ was forced to converge in the overall iteration to the fifth decimal. The interval of integration used was usually $\Delta\eta = 1/20$. Spot checks at intervals of $\Delta\eta = 1/40$ were consistent to the fourth decimal.

SOLUTIONS PRESENTED

Solutions are presented for systems wherein air is the ambient gas and H_2, He, H_2O (v) and CO_2 are introduced at the solid surface. Figures 3(a), (b) and (c) compare heat-transfer vs. mass-transfer rates as interpreted on different bases. The numbered curves in each of Figs. 4, 5, 6 and 7 represent

1. All properties held constant except for $\Lambda_{\rho ct}$ in the buoyancy term, with
$$\Lambda_{\rho ct} = \frac{T_{\infty}}{T}\left[X_A\left(\frac{M_A}{M_B} - 1\right) + 1\right].$$
2. Same as (1) except $\Lambda_{\rho c}$ is allowed to vary with concentration in the momentum equation, with
$$\Lambda_{\rho c} = X_A\left(\frac{M_A}{M_B} - 1\right) + 1.$$
3. Same as (2) except Λ_{C_p} is allowed to vary with concentration, with
$$\Lambda_{C_p} = \omega_A(C_{p_A}/C_{p_B} - 1) + 1.$$
4. Same as (3) except Λ_{μ} and Sc are allowed vary. The form used for Sc was
$$Sc = Sc_{\infty}\frac{\Lambda_{\mu}}{\Lambda_{\rho}\Lambda_D} = Sc_{\infty}\frac{\Lambda_{\mu}\Lambda_{\rho}}{\Lambda_{\rho}^2\Lambda_D} \cong Sc_{\infty}\frac{\Lambda_{\mu}\Lambda_{\rho c}}{\Lambda_{\rho ct}^2}$$
Λ_{μ} was calculated according to equation (6–26) of [14].
5. Same as (4) except Λ_k is allowed to vary with concentration. This represents the case wherein all properties are allowed to vary. Λ_k was calculated according to equation (7–22) of [14] for H_2–air, He–air and

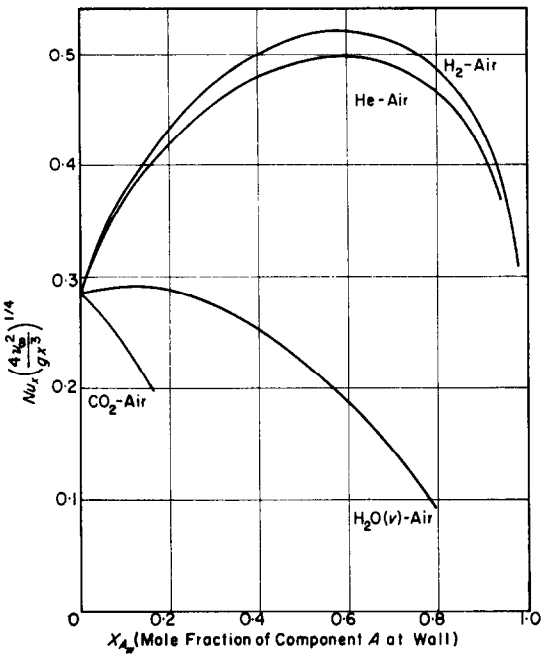

FIG. 3(a). Comparison of the relationship between heat transfer and mole fraction of component A at the wall for various binary systems. $T_w/T_\infty = 1{\cdot}1$

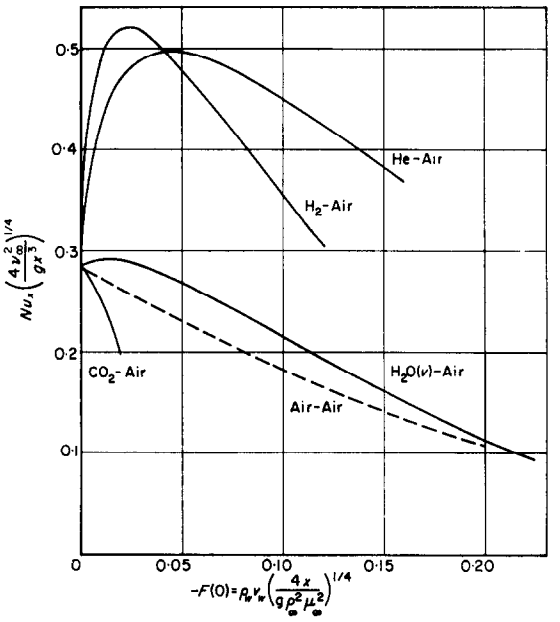

FIG. 3(b). Comparison of the relationship between heat transfer and mass flux at the wall for various binary systems. $T_w/T_\infty = 1{\cdot}1$.

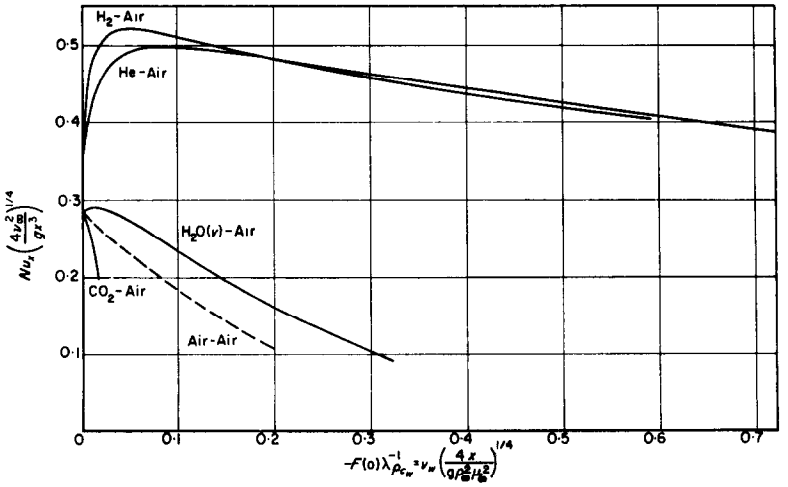

FIG. 3(c). Comparison of the relationship between heat transfer and interfacial velocity for various binary systems. $T_w/T_\infty = 1{\cdot}1$.

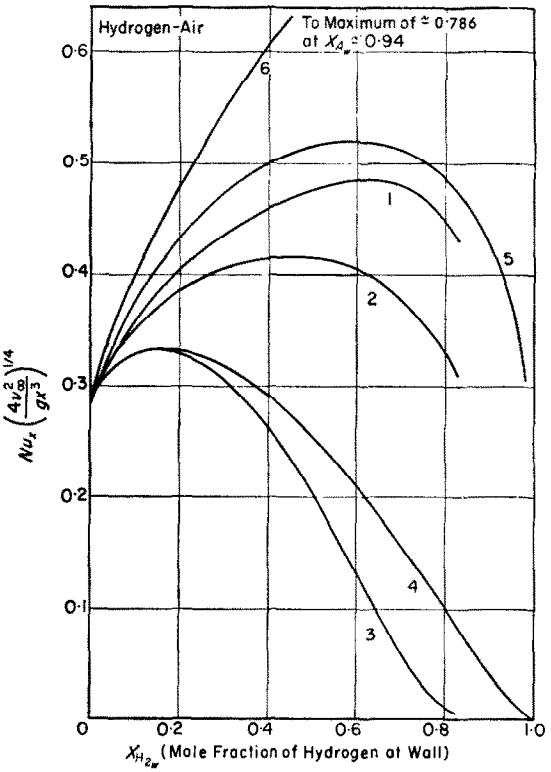

FIG. 4. Study of the effects of physical property variation on heat transfer for hydrogen–air system. See text, section entitled *Solutions Presented*, for key to curves. $T_w/T_\infty = 1{\cdot}1$.

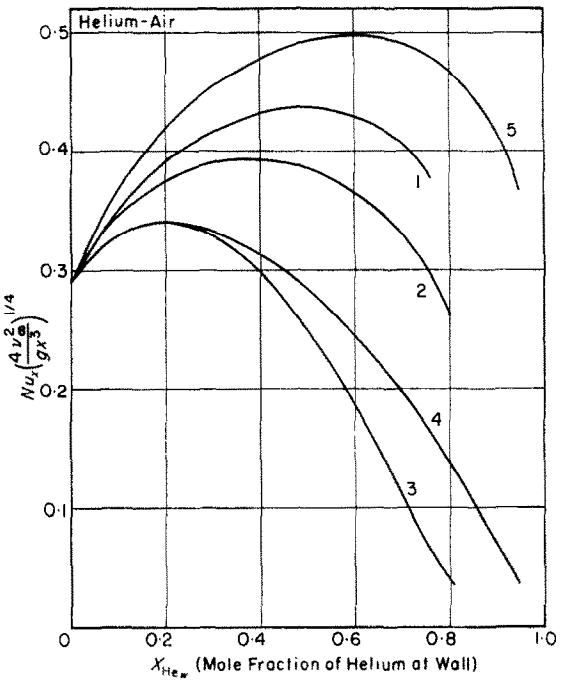

FIG. 5. Study of the effects of physical property variation on heat transfer for helium–air system. See text, section section entitled *Solutions Presented*, for key to curves. $T_w/T_\infty = 1{\cdot}1$.

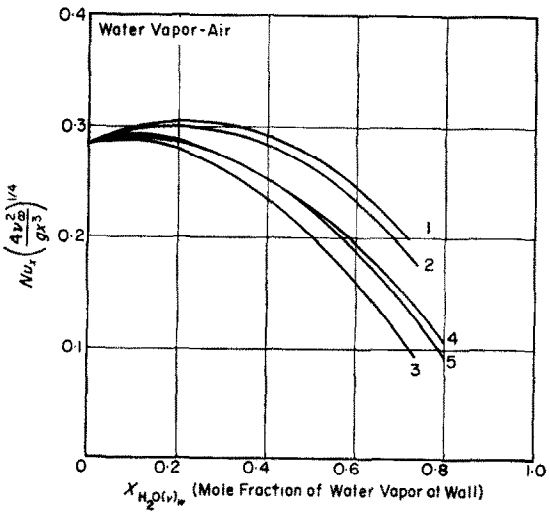

FIG. 6. Study of the effects of physical property variation on heat transfer for water vapor–air system. See text, section entitled *Solutions Presented*, for key to curves. $T_w/T_\infty = 1{\cdot}1$.

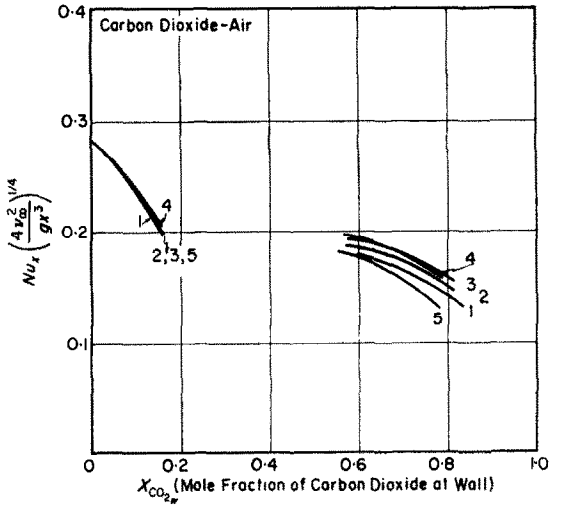

FIG. 7. Study of the effects of physical property variation on heat transfer for carbon dioxide–air system. See text, section entitled *Solutions Presented*, for key to curves. $T_w/T_\infty = 1{\cdot}1$.

CO_2–air, and equation (7–17) of [14] for H_2O (v)–air.

6. All properties are allowed to vary except Λ_{C_p}.

All properties, except $\Lambda_{\rho ct}$, were evaluated at 200°F. Data for curves 1 and 5 in Figs. 4, 5, 6, and 7 are presented in Table 1.

Figures 8 and 9 demonstrate the interaction of the interfacial velocity and the Prandtl number in a single component system. As mentioned in the analysis, these results are independent of T_w/T_∞.

Data for a two component liquid system are presented in Table 2. Note that in this case free convection is induced solely by thermal gradients, and that physical property variation is completely ignored.

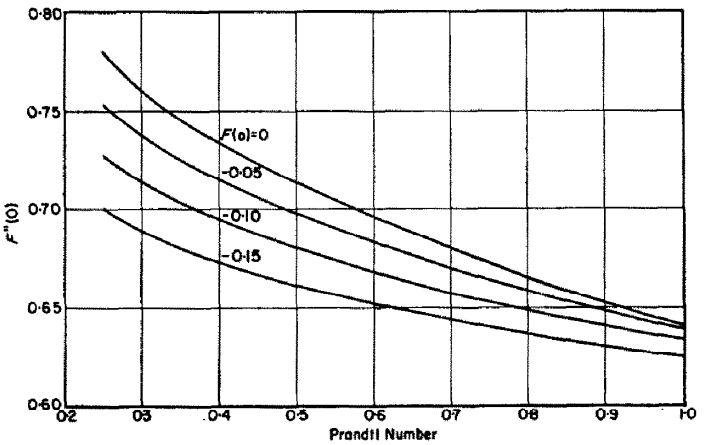

FIG. 8. Variation of dimensionless velocity gradient, $F''(0)$, with Pr at various transverse flow rates for a single component system.

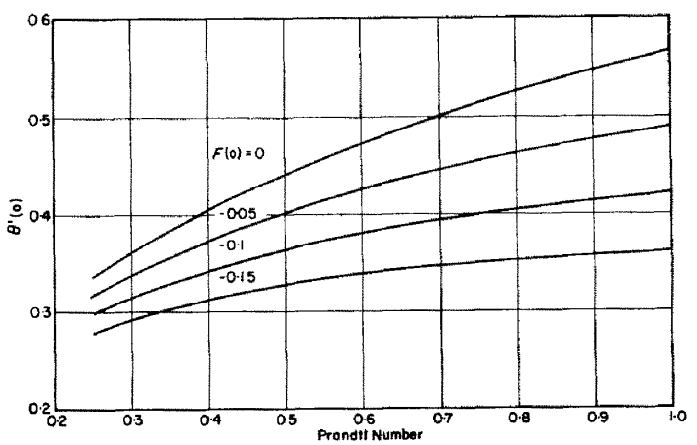

FIG. 9. Variation of dimensionless temperature gradient with Pr at various transverse flow rates for a single component system.

Table 1

Hydrogen–Air System: $Pr_\infty = 0{\cdot}72$, $Sc_\infty = 0{\cdot}25$, $\frac{M_A}{M_B} = 0{\cdot}069$, $\frac{T_w}{T_\infty} = 1{\cdot}1$

(curve 5, Fig. 4) $\frac{C_{pA}}{C_{pB}} = 14{\cdot}0$, $\frac{\mu_A}{\mu_B} = 0{\cdot}478$, $\frac{k_A}{k_B} = 6{\cdot}814$

$F(0)$	ω_{Aw}	X_{Aw}	$F''(0)$	$Sh_x\left[\frac{4\nu_\infty}{gx^3}\right]^{1/4}$	$Nu_x\left[\frac{4\nu_\infty}{gx^3}\right]^{1/4}$	$\Lambda_{\rho c t_w}$	$\Lambda_{\rho c_w}$	Λ_{μ_w}	Λ_{k_w}	$\Lambda_{C_{p_w}}$	Sc_w
0	0	0	0·1202	0·1522	0·2838	0·9091	1·0	1·0	1·0	1·0	0·3025
−0·001	0·0042	0·0575	0·1684	0·1783	0·3449	0·8604	0·9465	0·9986	1·193	1·054	0·3192
−0·0025	0·0096	0·1236	0·2104	0·1929	0·3930	0·8045	0·8850	0·9963	1·418	1·125	0·3405
−0·005	0·0183	0·2124	0·2499	0·2017	0·4400	0·7293	0·8023	0·9914	1·728	1·237	0·3738
−0·0075	0·0269	0·2862	0·2705	0·2034	0·4691	0·6668	0·7335	0·9853	1·994	1·350	0·4063
−0·01	0·0358	0·3500	0·2802	0·2020	0·4884	0·6129	0·6741	0·9783	2·230	1·465	0·4390
−0·015	0·0547	0·4562	0·2807	0·1945	0·5103	0·5230	0·5753	0·9612	2·645	1·711	0·5054
−0·025	0·0980	0·6117	0·2475	0·1726	0·5199	0·3914	0·4305	0·9173	3·324	2·274	0·6445
−0·04	0·1789	0·7596	0·1802	0·1377	0·4999	0·2662	0·2928	0·8368	4·129	3·326	0·8646
−0·06	0·3160	0·8701	0·1109	0·0974	0·4539	0·1726	0·1899	0·7270	4·971	5·108	1·158
−0·08	0·4747	0·9291	0·0706	0·0664	0·4036	0·1227	0·1350	0·6368	5·613	7·170	1·427
−0·10	0·6320	0·9614	0·0489	0·0437	0·3537	0·0954	0·1049	0·5729	6·077	9·216	1·652
−0·12	0·7654	0·9793	0·0372	0·0276	0·3050	0·0802	0·0882	0·5317	6·388	10·950	1·823
(curve 1, Fig. 4) $\frac{C_{pA}}{C_{pB}} = 1{\cdot}0$, $\frac{\mu_A}{\mu_B} = 1{\cdot}0$, $\frac{k_A}{k_B} = 1{\cdot}0$, density constant except in body-force term											
0	0	0	0·1202	0·1592	0·2838	0·9091	1·0	1·0	1·0	1·0	0·25
−0·001	0·0039	0·0540	0·1722	0·1906	0·3311	0·8634	0·9497				
−0·0025	0·0087	0·1131	0·2243	0·2132	0·3658	0·8134	0·8947				
−0·005	0·0157	0·1880	0·2862	0·2348	0·3987	0·7499	0·8249				
−0·0075	0·0221	0·2470	0·3327	0·2487	0·4193	0·7000	0·7701				
−0·01	0·0282	0·2959	0·3701	0·2588	0·4339	0·6587	0·7245				
−0·015	0·0396	0·3740	0·4283	0·2731	0·4534	0·5926	0·6518				
−0·025	0·0607	0·4839	0·5074	0·2900	0·4736	0·4995	0·5495				
−0·04	0·0901	0·5896	0·5797	0·3028	0·4842	0·4101	0·4511				
−0·06	0·1267	0·6778	0·6356	0·3102	0·4830	0·3354	0·3690				
−0·08	0·1612	0·7358	0·6679	0·3123	0·4741	0·2863	0·3149				
−0·10	0·1940	0·7773	0·6870	0·3116	0·4613	0·2512	0·2763				
−0·12	0·2254	0·8084	0·6975	0·3093	0·4462	0·2249	0·2474				
−0·14	0·2557	0·8328	0·7029	0·3057	0·4299	0·2042	0·2246				

Table 1—continued

Helium–Air System: $Pr_\infty = 0{\cdot}72$, $Sc_\infty = 0{\cdot}25$, $\frac{M_A}{M_B} = 0{\cdot}138$, $\frac{T_w}{T_\infty} = 1{\cdot}1$

(curve 5, Fig. 5) $\frac{C_{p_A}}{C_{p_B}} = 5{\cdot}132$, $\frac{\mu_A}{\mu_B} = 1{\cdot}075$, $\frac{k_A}{k_B} = 5{\cdot}4$

$F(0)$	ω_{A_w}	X_{A_w}	$F''(0)$	$Sh_x\left[\frac{4\nu_\infty}{gx^3}\right]^{1/4}$	$Nu_x\left[\frac{4\nu_\infty}{gx^3}\right]^{1/4}$	$\Lambda_{\rho c_{t_w}}$	$\Lambda_{\rho c_w}$	Λ_{μ_w}	Λ_{k_w}	$\Lambda_{C_{p_w}}$	Sc_w
0	0	0	0·1202	0·1522	0·2838	0·9091	1	1	1	1	0·3025
−0·002	0·0084	0·0581	0·1672	0·1764	0·3391	0·8636	0·9499	1·0080	1·1526	1·0348	0·3210
−0·005	0·0194	0·1252	0·2109	0·1899	0·3831	0·8110	0·8921	1·0175	1·3323	1·0800	0·3451
−0·0075	0·0280	0·1729	0·2366	0·1951	0·4076	0·7736	0·8510	1·0246	1·4623	1·1158	0·3642
−0·01	0·0365	0·2157	0·2564	0·1978	0·4262	0·7401	0·8141	1·0311	1·5810	1·1510	0·3831
−0·0150	0·0536	0·2909	0·2847	0·1989	0·4527	0·6811	0·7492	1·0430	1·7954	1·2213	0·4211
−0·025	0·0886	0·4136	0·3141	0·1928	0·4821	0·5850	0·6435	1·0631	2·1639	1·3663	0·4998
−0·04	0·1454	0·5523	0·3228	0·1763	0·4970	0·4762	0·5239	1·0863	2·6243	1·6009	0·6273
−0·06	0·2300	0·6841	0·3056	0·1507	0·4920	0·3730	0·4103	1·1059	3·1347	1·9504	0·8154
−0·08	0·3235	0·7761	0·2771	0·1255	0·4739	0·3009	0·3309	1·1150	3·5676	2·3366	1·0192
−0·1	0·4224	0·8413	0·2476	0·1026	0·4500	0·2497	0·2747	1·1163	3·9408	2·7454	1·2292
−0·12	0·5219	0·8878	0·2213	0·0824	0·4234	0·2133	0·2346	1·1127	4·2610	3·1566	1·4346
−0·15	0·6610	0·9339	0·1902	0·0577	0·3817	0·1772	0·1949	1·1036	4·6464	3·7311	1·7129
−0·16	0·7024	0·9448	0·1821	0·0509	0·3676	0·1687	0·1855	1·1004	4·7508	3·9023	1·7941

(curve 1, Fig. 5) $\frac{C_{p_A}}{C_{p_B}} = 1{\cdot}0$, $\frac{\mu_A}{\mu_B} = 1{\cdot}0$, $\frac{k_A}{k_B} = 1{\cdot}0$, density constant except in body-force term

0	0	0	0·1202	0·1592	0·2838	0·9091	1	1	1	1	0·25
−0·002	0·0079	0·0545	0·1688	0·1886	0·3273	0·8664	0·9530				
−0·005	0·0176	0·1147	0·2180	0·2099	0·3590	0·8192	0·9011				
−0·0075	0·0248	0·1556	0·2496	0·2213	0·3756	0·7871	0·8658				
−0·01	0·0316	0·1913	0·2762	0·2299	0·3878	0·7592	0·8351				
−0·02	0·0563	0·3020	0·3547	0·2513	0·4159	0·6724	0·7396				
−0·04	0·0998	0·4455	0·4483	0·2707	0·4347	0·5599	0·6159				
−0·07	0·1575	0·5754	0·5239	0·2808	0·4331	0·4581	0·5039				
−0·1	0·2099	0·6582	0·5645	0·2824	0·4187	0·3933	0·4326				
−0·12	0·2426	0·6990	0·5810	0·2810	0·4059	0·3613	0·3974				
−0·14	0·2738	0·7322	0·5918	0·2784	0·3916	0·3353	0·3688				
−0·16	0·3038	0·7598	0·5983	0·2750	0·3764	0·3136	0·3450				

Table 1—continued

Water Vapor–Air System: $Pr_\infty = 0{\cdot}72$, $Sc_\infty = 0{\cdot}45$, $\frac{M_A}{M_B} = 0{\cdot}621$, $\frac{T_w}{T_\infty} = 1{\cdot}1$

(curve 5, Fig. 6) $\frac{C_{p_A}}{C_{p_B}} = 1{\cdot}988$, $\frac{\mu_A}{\mu_B} = 0{\cdot}588$, $\frac{k_A}{k_B} = 0{\cdot}778$

$F(0)$	ω_{A_w}	X_{A_w}	$F''(0)$	$Sh_x\left[\frac{4\nu_\infty}{gx^3}\right]^{1/4}$	$Nu_x\left[\frac{4\nu_\infty}{gx^3}\right]^{1/4}$	$\Lambda_{\rho c_{t_w}}$	$\Lambda_{\rho c_w}$	Λ_{μ_w}	Λ_{k_w}	$\Lambda_{C_{p_w}}$	Sc_w
0	0	0	0·1202	−0·2098	−0·2838	0·9091	1·0000	1·0000	1·0000	1·0000	0·5445
−0·002	0·0125	0·0200	0·1252	−0·2127	−0·2866	0·9022	0·9924	0·9918	1·0022	1·0124	0·5442
−0·005	0·0303	0·0480	0·1316	−0·2160	−0·2895	0·8926	0·9818	0·9804	1·0047	1·0299	0·5437
−0·0075	0·0444	0·0696	0·1360	0·2180	0·2909	0·8851	0·9736	0·9715	1·0062	1·0439	0·5433
−0·0100	0·0579	0·0902	0·1398	0·2195	0·2917	0·8780	0·9658	0·9631	1·0072	1·0572	0·5430
−0·0250	0·1315	0·1962	0·1545	0·2228	0·2882	0·8415	0·9256	0·9196	1·0078	1·1300	0·5410
−0·0500	0·2361	0·3325	0·1625	0·2184	0·2683	0·7945	0·8739	0·8637	0·9968	1·2333	0·5381
−0·075	0·3282	0·4405	0·1620	0·2072	0·2423	0·7572	0·8329	0·8192	0·9793	1·3243	0·5355
−0·100	0·4094	0·5276	0·1573	0·1947	0·2139	0·7272	0·7999	0·7833	0·9598	1·4045	0·5332
−0·125	0·4830	0·6008	0·1510	0·1807	0·1865	0·7019	0·7721	0·7531	0·9398	1·4772	0·5311
−0·150	0·5488	0·6622	0·1439	0·1665	0·1599	0·6808	0·7488	0·7278	0·9207	1·5422	0·5292
−0·200	0·6612	0·7587	0·1294	0·1383	0·1126	0·6475	0·7122	0·6879	0·8862	1·6533	0·5259
−0·225	0·7087	0·7968	0·1224	0·1248	0·0924	0·6343	0·6978	0·6722	0·8712	1·7002	0·5245
(curve 1, Fig. 6) $\frac{C_{p_A}}{C_{p_B}} = 1{\cdot}0$, $\frac{\mu_A}{\mu_B} = 1{\cdot}0$, $\frac{k_A}{k_B} = 1{\cdot}0$, density constant except in body-force term											
0	0	0	0·1202	0·2222	0·2838	0·9091	1	1	1	1	0·4500
−0·002	0·0118	0·0189	0·1271	0·2259	0·2879	0·9026	0·9928				
−0·005	0·0285	0·0451	0·1364	0·2305	0·2927	0·8936	0·9829				
−0·0075	0·0415	0·0653	0·1435	0·2336	0·2958	0·8866	0·9752				
−0·01	0·0541	0·0843	0·1500	0·2362	0·2983	0·8800	0·9680				
−0·025	0·1209	0·1814	0·1815	0·2453	0·3052	0·8465	0·9312				
−0·05	0·2135	0·3042	0·2173	0·2487	0·3025	0·8042	0·8846				
−0·075	0·2918	0·3990	0·2419	0·2457	0·2924	0·7715	0·8487				
−0·1	0·3603	0·4758	0·2596	0·2397	0·2789	0·7450	0·8195				
−0·125	0·4213	0·5398	0·2723	0·2318	0·2636	0·7230	0·7953				
−0·15	0·4761	0·5941	0·2815	0·2229	0·2475	0·7042	0·7746				
−0·2	0·5705	0·6815	0·2918	0·2033	0·2146	0·6741	0·7415				
−0·225	0·6114	0·7171	0·2940	0·1931	0·1984	0·6618	0·7280				

Table 1—continued

Carbon Dioxide–Air System: $Pr_\infty = 0{\cdot}72$, $Sc_\infty = 1{\cdot}15$, $\frac{M_A}{M_B} = 1{\cdot}517$, $\frac{T_w}{T_\infty} = 1{\cdot}1$

(curve 5, Fig. 7) $\frac{C_{p_A}}{C_{p_B}} = 0{\cdot}930$, $\frac{\mu_A}{\mu_B} = 0{\cdot}845$, $\frac{k_A}{k_B} = 0{\cdot}731$

$F(0)$	ω_{Aw}	X_{Aw}	$F''(0)$	$Sh_x\left[\frac{4\nu_\infty}{gx^3}\right]^{1/4}$	$Nu_x\left[\frac{4\nu_\infty}{gx^3}\right]^{1/4}$	$\Lambda_{\rho c t_w}$	Λ_{c_w}	Λ_{μ_w}	Λ_{k_w}	$\Lambda_{C_{p_w}}$	Sc_w
0	0	0	0·1201	0·3280	0·2838	0·9091	1	1	1	1	1·392
−0·005	0·0527	0·0354	0·1056	0·3102	0·2682	0·9257	1·018	0·9929	0·9888	0·9963	1·357
−0·01	0·1067	0·0730	0·0889	0·2888	0·2503	0·9434	1·038	0·9855	0·9771	0·9925	1·321
−0·0125	0·1350	0·0933	0·0794	0·2762	0·2399	0·9530	1·048	0·9816	0·9709	0·9905	1·303
−0·015	0·1652	0·1154	0·0684	0·2615	0·2277	0·9633	1·060	0·9774	0·9641	0·9884	1·283
−0·0175	0·1994	0·1410	0·0546	0·2425	0·2121	0·9754	1·073	0·9726	0·9564	0·9860	1·261
−0·019	0·2255	0·1610	0·0428	0·2252	0·1980	0·9848	1·083	0·9689	0·9504	0·9842	1·245
				Change in geometry—see discussion							
−0·125	0·6655	0·5673	0·1827	0·2168	0·1804	1·176	1·293	0·9020	0·8373	0·9534	0·9704
−0·150	0·7135	0·6214	0·2020	0·2078	0·1727	1·201	1·321	0·8942	0·8234	0·9501	0·9416
−0·175	0·7541	0·6691	0·2175	0·1968	0·1633	1·224	1·346	0·8875	0·8112	0·9472	0·9175
−0·200	0·7888	0·7111	0·2299	0·1848	0·1530	1·243	1·368	0·8817	0·8007	0·9448	0·8970
−0·2250	0·8185	0·7482	0·2397	0·1721	0·1423	1·261	1·387	0·8767	0·7914	0·9427	0·8795
−0·250	0·8441	0·7811	0·2470	0·1593	0·1314	1·276	1·404	0·8723	0·7833	0·9409	0·8645

(curve 1, Fig. 7) $\frac{C_{p_A}}{C_{p_B}} = 1{\cdot}0$, $\frac{\mu_A}{\mu_B} = 1{\cdot}0$, $\frac{k_A}{k_B} = 1{\cdot}0$, density constant except in body-force term

0	0	0	0·1202	0·3554	0·2838	0·9091	1·0	1·0	1·0	1·0	1·15
−0·005	0·0492	0·0330	0·1057	0·3313	0·2683	0·9246	1·017				
−0·01	0·1007	0·0687	0·0893	0·3080	0·2506	0·9414	1·036				
−0·0125	0·1280	0·0882	0·0799	0·2937	0·2404	0·9506	1·046				
−0·015	0·1572	0·1095	0·0694	0·2774	0·2287	0·9606	1·057				
−0·0175	0·1901	0·1340	0·0565	0·2572	0·2140	0·9721	1·069				
−0·019	0·2141	0·1522	0·0463	0·2407	0·2019	0·9807	1·079				
				Change in geometry—see discussion							
−0·125	0·6938	0·5990	0·1785	0·1903	0·1780	1·191	1·310				
−0·150	0·7461	0·6595	0·1974	0·1761	0·1715	1·219	1·341				
−0·175	0·7898	0·7124	0·2127	0·1607	0·1629	1·244	1·368				
−0·200	0·8264	0·7583	0·2248	0·1449	0·1533	1·266	1·392				
−0·225	0·8571	0·7980	0·2343	0·1295	0·1432	1·284	1·413				
−0·250	0·8827	0·8322	0·2415	0·1147	0·1328	1·300	1·430				

Table 2. Liquid system: $Pr_\infty = 10$, $Sc_\infty = 500$

Free convection due to concentration gradients ignored. Physical properties held constant.

$F(0)$	ω_{Aw} (if $\omega_{A\infty} = 0$)	$-F''(0)$	$Sh_x\left[\frac{4}{Gr_x}\right]^{1/4}$	$Nu_x\left[\frac{4}{Gr_x}\right]^{1/4}$
0	0	0·4192	5·045	1·169
−0·0002	0·0580	0·4195	4·876	1·167
−0·0004	0·1130	0·4198	4·711	1·164
−0·0008	0·2147	0·4205	4·390	1·157
−0·0015	0·3689	0·4216	3·859	1·147
−0·0025	0·5418	0·4231	3·171	1·132
−0·01	0·9722	0·4342	0·4297	1·035

DISCUSSION

This work is concerned with the study of physical property variation with concentration and the resultant effects on heat, mass and momentum transfer. Clearly, in a binary system where a pure foreign fluid is being injected into a pure ambient fluid, if the properties of the two fluids are significantly different then the concentration variation will result in pronounced variation of such properties as thermal conductivity, heat capacity, density and viscosity. The effects of these properties on heat, mass and momentum transfer are nonlinear, so that, short of making calculations for every conceivable system, one can only extract as much information as possible from a detailed treatment of a few systems, and hopefully, derive more general approximate solutions or develop suitable correlation techniques.

Perhaps the most critical assumption of this work, in the light of recently published research, is that of neglecting the effects of Soret–Dufour diffusion. Sparrow *et al.* [10, 11] in studies of binary systems have found that these effects can be quite pronounced, especially in free convection systems wherein the entrant foreign material is of low molecular weight relative to the ambient fluid. However, the same workers also indicated that experimental data can be correlated reasonably well with calculations which neglect Soret–Dufour diffusion, at least for the case of free convection stagnation flow, by basing the experimental Nusselt number on the temperature difference $T_w - T_{aw}$ rather than $T_w - T_\infty$, where T_{aw} is the adiabatic wall temperature. Hence, the calculations in the present paper for hydrogen and helium which neglected thermodynamic coupling have practical significance as well as value in studying the relative effects of physical property variation with concentration.

As stated in the analysis, another assumption of this study is that the quantities Λ_{C_p}, $\Lambda_\mu\Lambda_\rho$ and Λ_k/Λ_μ are assumed to be independent of temperature. To test this assumption calculations were made for temperature ratios of interest for the free convection stagnation flow problem, and, as indicated in Fig. 2, the results obtained are in good agreement with the temperature-dependent results obtained by Sparrow *et al.* [11]. The assumption, of course, becomes progressively worse if T_w/T_∞ deviates very significantly from unity.

It is worth noting the striking changes in the appearances of the heat-transfer results when plotted on different bases. In Figs. 3(a), (b) and (c), for example, the heat-transfer rate is plotted vs. mole fraction of component A at the surface, mass flux at the surface, and interfacial velocity, respectively. In each of these the results have a markedly different appearance, so that one must be careful to specify the basis when comparing the heat-transfer effects of various coolants.

The predicted heat-transfer rates for the H_2, He, and H_2O air systems increase at low mass-transfer rates, then decrease at higher rates. For He and H_2 the initial increase is due primarily to two factors. First, both components have molecular weights less than that of air, so that concentration-induced buoyancy effects augment the convection (when $T_w/T_\infty > 1$), thereby increasing heat transfer. Also, the thermal conductivities of He and H_2 are greater than that

of air, so that increasing the amount of He and H_2 in the boundary layer augments heat-transfer rates. It is apparent from Figs. 4 and 5 that the latter is the largest factor for these components, since the increase is far less when the effect of thermal conductivity is ignored.

The decrease in heat transfer at higher mass-transfer rates for the He and H_2 air systems may also be largely attributed to two factors. First, the heat capacities of these substances are greater than that of air, so that more heat is "absorbed" as the mass fractions of He and H_2 increase. Also, the transverse velocity tends to increase the thickness of the boundary layer, thereby increasing resistance to heat transfer.

It is perhaps worth noting that for systems wherein M_A/M_B is significantly different from unity the thermal conductivity variation will be more pronounced at a different level of mass transfer than will heat capacity variation. This occurs because thermal conductivity varies more directly with the mole fraction of component A, whereas heat capacity varies with the mass fraction. For example, in the case of the H_2 air system, wherein $M_A/M_B \cong 0{\cdot}069$, the mole fraction of hydrogen increases much more rapidly than does the mass fraction at low mass-transfer rates. Hence, in this region the thermal conductivity varies rapidly, while the heat capacity is almost constant. The reverse occurs at higher mass-transfer rates, when the mole fraction increases more slowly than does the mass fraction. (Compare curves 4, 5 and 6 in Fig. 4).

It must, of course, be borne in mind that in any case the effect on heat transfer of variation in properties with concentration will depend in large measure on the relative thickness of the thermal and diffusion boundary layers, the magnitude of the effect increasing with the ratio of the latter to the former.

Since the thermal conductivity of H_2O is slightly less than that of air, the increase in heat transfer at low mass-transfer rates must be due solely to the concentration-induced buoyancy effects. At higher rates the thermal conductivity, heat capacity and boundary-layer thickening effects predominate, thereby reducing heat transfer.

Figures 4 and 5 indicate that the effects of physical property variations in the H_2 and He air systems are quite similar, the most pronounced being, by far, those of heat capacity and thermal conductivity. We see from Fig. 6, on the other hand, that property variations for the H_2O air system are much less pronounced, but of the same general nature as the H_2 and He air systems, with one important exception. The thermal conductivity of H_2O is slightly less than that of air, as evidenced by the downward shift from curve 4 to curve 5, which enhances the attractiveness of H_2O as a coolant material.

An interesting observation from Figs. 4 and 5 is that the best approximation to the case where all properties vary is that where none vary; this implies, at least for the He and H_2 air systems, that the effects of property variation with concentration tend to cancel. This is not true for the highly polar H_2O–air system.

For CO_2, Fig. 7, the effects of physical property variation with concentration are seen to be relatively slight. The primary consideration here is that of concentration-induced buoyancy effects which oppose the thermally induced buoyancy effects (when $T_w/T_\infty > 1$) and thereby reduce the convection rate and inhibit heat transfer. Note that the curves for the CO_2 air system terminate, then begin again. This occurs since the molecular weight of CO_2 is greater than that of air, and at a certain mass-transfer rate the buoyancy effects due to concentration gradients overcome those due to thermal gradients (when $T_w/T_\infty > 1$) and the flow reverses. At this point boundary-layer theory requires that the analysis change from consideration of a flat plate with leading edge downward to a flat plate with leading edge upward. Hence, the separated segments of the curves in Fig. 7 are not really directly related, but refer to different systems.

Some useful information can be derived by considering a single-component system. In particular, the behavior of the shear stress and Nusselt number as functions of $F(0)$ and Pr is shown in Figs. 8 and 9 for gaseous systems. Clearly, heat transfer is more significantly affected by transverse flow than is momentum transport. It is seen that $F''(0)$ decreases as the blowing velocity increases and also as Pr increases. In contrast, $\theta'(0)$ increases with Pr and decreases with increased blowing. Furthermore,

changes in $F''(0)$ with $F(0)$ are most pronounced at lower values of Pr. It seems particularly interesting that $F''(0)$ is more responsive to transverse convection at lower values of Pr.

Data for a liquid system with $Pr = 10$ and $Sc = 500$ are summarized in Table 2. These solutions are typical of a number of liquid systems since the Lewis number, Sc/Pr, is significantly greater than one. When the Lewis number is large, as in this case, free convection will most often be caused almost completely by thermal effects since the diffusion boundary layer is much thinner than the thermal boundary layer. Consequently, this was the case studied here. Because of the high resistance to mass transfer at $Sc = 500$, a rather large difference between wall and free stream mass fractions is necessary to maintain the very small mass-transfer rates studied here. In this case the only significant change occurs in $\phi'(0)$, and and it is quite natural that $\phi'(0)$ should be the most sensitive to $F(0)$, again because of the large value of Sc.

ACKNOWLEDGEMENTS

This work was sponsored by the Office of Naval Research under Contract NONR-669(17). The authors also are indebted to the Syracuse University Computing Center for the use of their facilities.

REFERENCES

1. A. Acrivos, *Chem. Engng Sci.* **17**, 457 (1962).
2. E. R. G. Eckert and T. W. Jackson, *NACA* Report 1015 (1951).
3. R. Eichhorn, *J. Heat Transfer*, **82**, 260 (1960).
4. H. Nakamura, *Bull. Japan Soc. Mech. Engrs* **5**, 311 (1962).
5. S. Ostrach, Nat'l. Advisory Comm. Aeronaut., Report 1111 (1953).
6. M. G. Scherberg, *Int. J. Heat Mass Transfer* **5**, 1001 (1962).
7. E. V. Somers, *J. Appl. Mech.* **23**, 295 (1956).
8. E. M. Sparrow and J. L. Gregg, *Trans. Amer. Soc. Mech. Engrs.* **80**, 379 (1958); **80**, 879 (1958).
9. E. M. Sparrow and R. D. Cess, *J. Heat Transfer* **83**, 387 (1961).
10. E. M. Sparrow, W. J. Minkowycz and E. R. G. Eckert, *AIAA J.* **2**, 652 (1964).
11. E. M. Sparrow, W. J. Minkowycz and E. R. G. Eckert, ASME Paper 63-*WA*-50.
12. Kwang-Tzu Yang and E. W. Jerger, *J. Heat Transfer* **86**, 107 (1964).
13. D. W. Zeh and W. N. Gill Binary diffusion and heat transfer in laminar boundary layers on vertical surfaces, *Seventh National Heat Transfer Conference*, A.I.Ch.E. Preprint 28 (August 1964).
14. R. C. Reid and T. K. Sherwood, *The Properties of the Gases and Liquids*. McGraw-Hill, New York (1958).

Résumé—On a étudié des couches limites laminaires de convection libre avec des transports couplés de quantité de mouvement, de chaleur et de masse binaire en fonction des paramètres agissants. Les effets de poussée d'Archimède produits à la fois par les gradients de température et de concentration ont été considérés. On a recherché des solutions exactes du système non-linéaire des trois équations couplées pour des systèmes à propriétés physiques variables avec une force d'Archimède constante parallèle à la surface solide, pour beaucoup de cas différents afin d'obtenir une idée raisonnable de la façon dont les différents paramètres influent sur les processus de transport en cause.

Les effets des variations avec la concentration des enthalpies des constituants, de la conductivité thermique, de la viscosité et de la densité ont été étudies individuellement et dans diverses combinaisons. Les effets les plus frappants sont ceux produits par les différences d'enthalpie de constituants et par la conductivité thermique pour les gaz de poids moléculaire faible. On a recherché également les interactions du nombre de Prandtl et des effets de la vitesse interfaciale pour des systèmes de transfert de masse avec un seul constituant.

Une méthode d'intégration des équations de transport couplées a été exposée et elle semble être considérablement plus rapide que les techniques employées auparavant. L'amélioration de la vitesse de calcul se produit principalement parce que chaque solution de l'équation de quantité de mouvement est obtenue en itérant seulement sur une condition à la limite plutôt que de le faire à la fois sur une condition à la limite et une fonction comme els méthodes antérieures le demandent.

Zusammenfassung—Die freie Konvektion in laminaren Grenzschichten mit gekoppeltem Impuls-, Wärme- und Zweistoffaustausch wurde in Termen der massgebenden Parameter berechnet. Auftriebseinflüsse, die sowohl von Temperatur- als auch von Konzentrationsgradienten herrühren, wurden berücksichtigt. Für viele verschiedene Fälle wurden die genauen Lösungen des nichtlinearen Systems dreier gekoppelter Gleichungen für variable physikalische Stoffwertsystem mit konstanter Massenkraft parallel zu der festen Oberfläche untersucht, um eine brauchbare Vorstellung über den Einfluss der verschiedenen Parameter auf die Übergangsvorgänge zu bekommen.

Insbesondere wurden die Auswirkungen von Änderungen der Enthalpie, des Wärmeleitvermögens, der Zähigkeit und der Dichte mit der Konzentration einzeln und in verschiedenen Kombinationen untersucht. Der grösste Einfluss kommt von Unterschieden der Enthalpie und des Wärmeleitvermögens bei Gasen mit niedrigem Molekulargewicht. Auch die Wechselwirkungen der Prandtl-Zahl und die Einflüsse der Grenzflächengeschwindigkeit für Stoffübergangssysteme mit einer einzelnen Komponente wurden untersucht.

Für die gekoppelten Transportgleichungen wurden eine Integrationsmethode entwickelt, die wesentlich schneller zum Ziel zu führen scheint als bisher verwendete Techniken. Die grössere Berechnungsgeschwindigkeit ergibt sich hauptsächlich deswegen, weil man jede Lösung der Impulsgleichung durch Iterieren von nur einer Grenzschichtbedingung anstatt wie bisher von einer Grenzschichtbedingung und einer Funktion, erhält.

Аннотация—Свободная конвекция в ламинарных пограничных слоях при наличии переноса количества движения, тепла и массообмена в бинарной смеси исследовалась в зависимости от соответствующих параметров. Рассмотрены эффекты пловучести, вызванные как градиентами температуры, так и концентрации. Точные решения нелинеинои системы трех связанных уравнений для системы с переменными физическими свойствами при постоянной генерируемой объемной силе, параллельной поверхности твердого тела были исследованы для многих случаев, чтобы получить соответствующее представление о том, как различные параметры влияют на процессы переноса, действующие в данных случаях.

Влияние изменений энтальпии, теплопроводности, вязкости и плотности компонент с концентрацией исследовались отдельно и в различных комбинациях. Наиболее сильное влияние оказывают изменения энтальпии и теплопроводности для газов с низким молекулярным весом. Также исследовались взаимодействия числа Прандтля и влияний скоростей на границе раздела фаз для систем с однокомпонентным массообменом. Был разработан метод интегрирования связанных уравнений переноса, использование которого дает результаты существенно быстрее, чем ранее используемые методы.

Увеличенная скорость расчета происходит в основном, потому что каждое решение уравнения количества движения получено итерированием только граничного условия, а не граничного условия и функции, как это требовалось в ранее используемых методах.